Structural Engineering and Mechanics, *Vol. 60, No. 2 (2016) 337-350*
DOI: http://dx.doi.org/10.12989/sem.2016.60.2.337

Assessment of steel components and reinforced concrete structures under steam explosion conditions

Seung Hyun Kim[1], Yoon-Suk Chang[*1] and Yong-Jin Cho[2]

[1]*Department of Nuclear Engineering, Kyung Hee University, 1732 Deogyeong-daero, Giheung-gu, Yongin-si, Gyeonggi-do, 17104, Republic of Korea*
[2]*Korea Institute of Nuclear Safety, 62 Gwahak-ro, Yuseong-gu, Daejeon-si, 34142, Republic of Korea*

(Received March 20, 2016, Revised July 18, 2016, Accepted July 28, 2016)

Abstract. Even though extensive researches have been performed for steam explosion due to their complex mechanisms and inherent uncertainties, establishment of severe accident management guidelines and strategies is one of state-of-the arts in nuclear industry. The goal of this research is primarily to examine effects of vessel failure modes and locations on nuclear facilities under typical steam explosion conditions. Both discrete and integrated models were employed from the viewpoint of structural integrity assessment of steel components and evaluation of the cracking and crushing in reinforced concrete structures. Thereafter, comparison of systematic analysis results was performed; despite the vessel failure modes were dominant, resulting maximum stresses at the all steel components were sufficiently lower than the corresponding yield strengths. Two failure criteria for the reinforced concrete structures such as the limiting failure ratio of concrete and the limiting strains for rebar and liner plate were satisfied under steam explosion conditions. Moreover, stresses of steel components and reinforced concrete structures were reduced with maximum difference of 12% when the integrated model was adopted comparing to those of discrete models.

Keywords: containment wall penetration; finite element analysis; main piping; reactor cavity; steam explosion

1. Introduction

In order to mitigate hypothetical severe accident scenarios in an advanced light water reactor, either core catcher or ERVC (External Reactor Vessel Cooling) strategy is adopted during design stage. However, when molten core penetrates RPV (Reactor Pressure Vessel) lower plenum and contacts with water in the reactor cavity, serious structural damage may occur. The steam explosion can lead to the formation of pressure waves and production of fragments may threaten the surrounding reactor cavity and associated components due to resulting dynamic effects (Kim *et al*. 2015, Cizelj *et al*. 2010). The expansion of high pressure mixture against inertial constraints imposed by the surroundings governs potential of the steam explosion. If the localized high pressure is quickly stabilized, only the kinetic energy transmitted to the materials around the interaction zone becomes the sole damaging agent.

*Corresponding author, Professor, E-mail: yschang@khu.ac.kr

http://www.techno-press.org/?journal=sem&subpage=8 ISSN: 1225-4568 (Print), 1598-6217 (Online)

Lots of researches have been carried out to study the steam explosion phenomenon and process. For instance, a reactor cavity was assessed by using a FE (Finite Element) code with the pressure waves obtained by a CFD (Computational Fluid Dynamics) code (Cizelj *et al*. 2006). Dynamic pressure loads were estimated and stresses of containment wall were calculated by the equivalent concrete structures. As another study, integrity of containment building of a CPR1000 was assessed under typical scenarios of steam explosions by using FE model (Chunyu *et al*. 2014). Three-dimensional FE models were set up to investigate dynamic response and the possible damage of containment wall. However, quantitative assessment of complex assembled model of steel components and reinforced structures has rarely been attempted in the previous researches.

The goal of this research is primarily to examine effects of RPV failure modes and locations on nuclear facilities such as steel components and reinforced concrete structures under typical steam explosion conditions. Both discrete and integrated models were employed from the viewpoint of structural integrity assessment of steel components and evaluation of the cracking and crushing in reinforced concrete structures. Fig. 1 represents the schematic of steam explosion process and explosion locations considered in the present study. Characteristics of the integrated model as well as the discrete models A (RPV, reactor coolant piping and reactor cavity) and B (steam generator, main steam piping and containment wall penetration) are explained in the following section 2. Resulting cracking, crushing, stresses and displacements are compared and their details are discussed in sections 3 and 4.

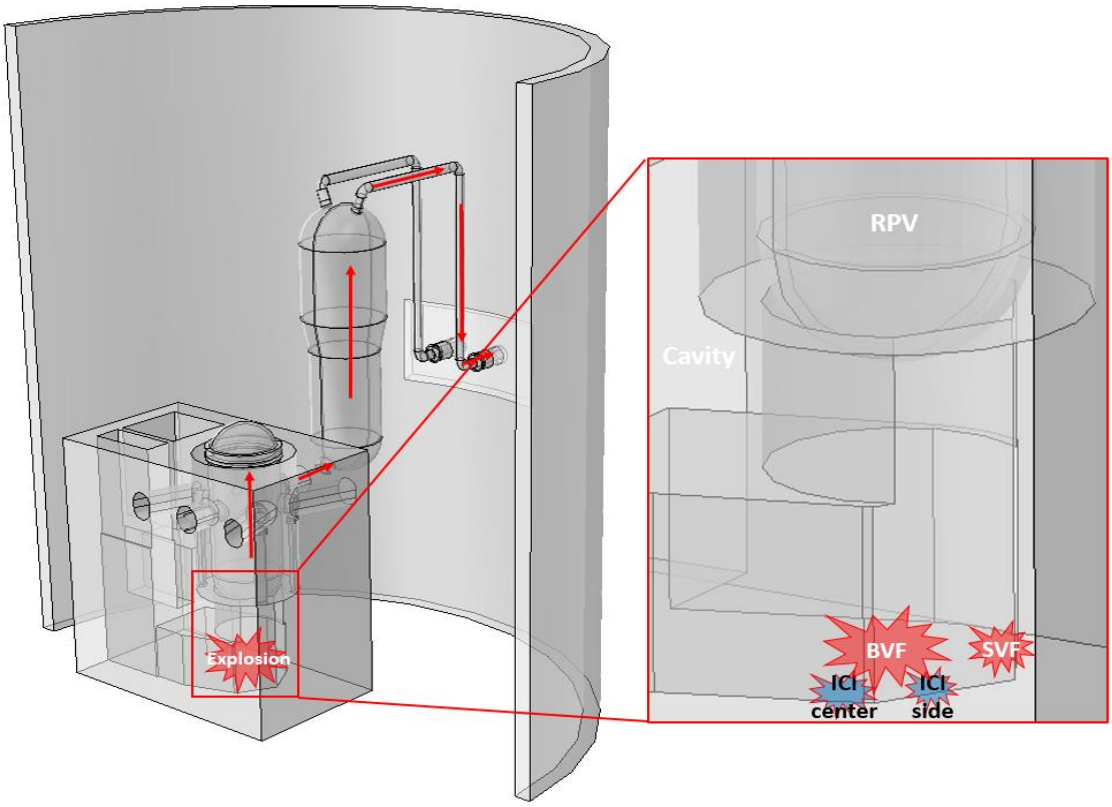

Fig. 1 Schematic of steam explosion process and explosion locations

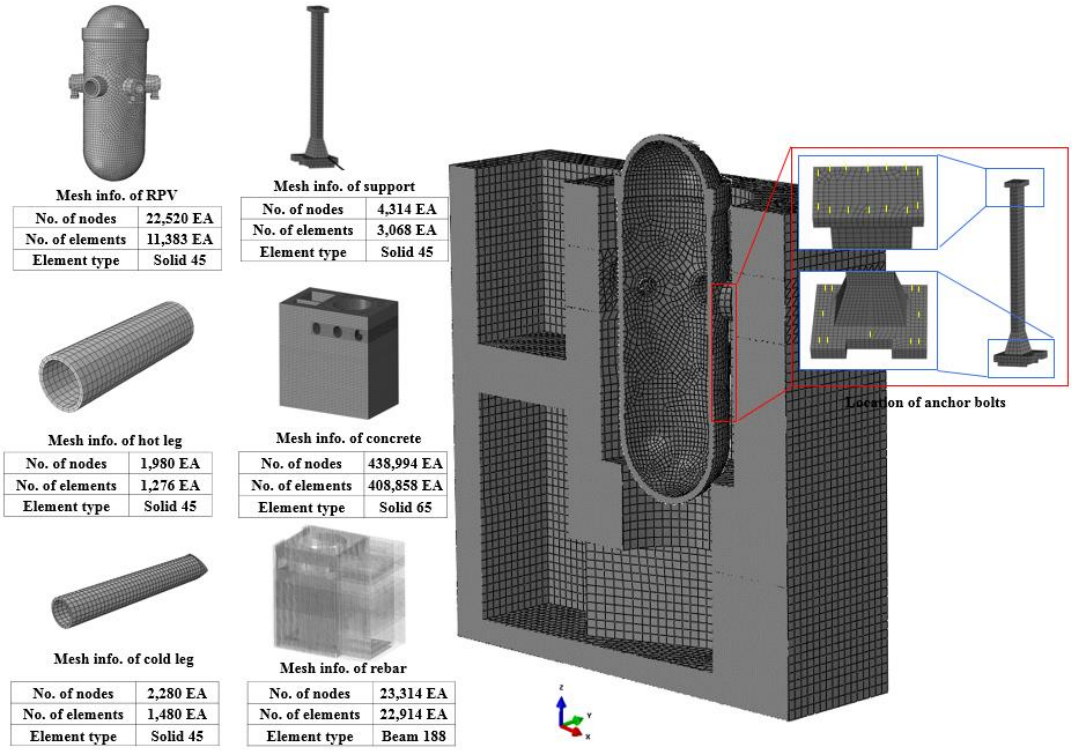

Fig. 2 Discrete FE model of RPV, reactor coolant piping and reactor cavity

2. Characteristics of descrete and integrated models

2.1 RPV, reactor coolant piping and reactor cavity

The discrete model A of RPV, reactor coolant piping and reactor cavity are illustrated in Fig. 2 for the steam explosion analyses. The reactor cavity was modeled by employing 8-node 3D concrete elements. Number of nodes was 438,994 and number of elements was 408,858. The steel liner plate was modeled by shell elements and merged with the concrete. The vertical and horizontal rebar embedded in the concrete were modeled by using beam elements. The RPV was modeled by employing 8-node solid elements with 20,620 nodes and 10,282 elements. Also, support structures were modeled by the same solid elements consisting 4,313 nodes and 3,068 elements. 10 anchor bolts per each support were modeled by 4 node beam elements with equivalent diameter. Cold leg and hot leg pipes were modeled by the 8-node solid elements with 1,480 and 1,276 elements as well as 2,280 and 1,980 nodes, respectively (Kim *et al*. 2015). Element types of each components were employed from general-purpose commercial program element library (ANSYS Civil FEM 2015).

2.2 SG, main steam piping and containment wall penetration

The discrete model B of SG (Steam Generator), main steam piping and containment wall

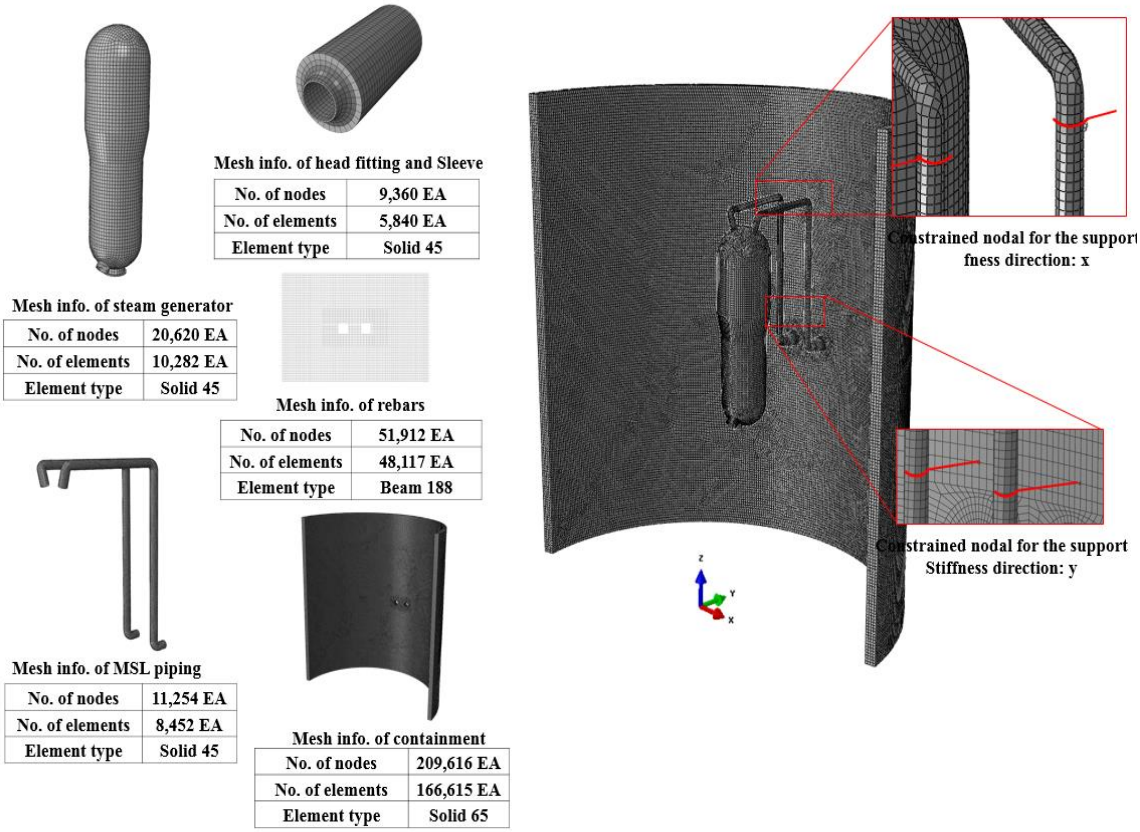

Fig. 3 Discrete FE model of SG, main steam piping and containment wall penetration

penetration used for the steam explosion analyses are illustrated in Fig. 3. The containment wall was modeled by employing 8-node 3D concrete elements. Number of nodes was 209,616 and number of elements was 166,615. The steel liner plate was modeled by employing shell elements and merged with the concrete. The vertical and horizontal rebar embedded in the concrete were modeled by using beam elements. The SG was modeled by employing 8-node solid elements with 20,620 nodes and 10,282 elements. Also, head fitting and sleeve were modeled by same solid elements consisting 9,360 nodes and 5,840 elements. Main steam piping were generated by 8-node solid elements with 11,254 and 8,452 elements, respectively (Kim *et al*. 2015). Element types of each component were employed from general-purpose commercial program element library (ANSYS Civil FEM 2015).

2.3 Integration of two discrete models

In order to confirm further realistic behaviors of the discrete models shown in Figs. 2 and 3, an integrated model was generated by combining the two discrete models. Since parts of the integrated model were the same with the discrete models themselves, mesh information of each component and reinforced structures was identical. It consists of 796,164 nodes and 688,285, respectively, of the integrated model.

3. Numerical analysis

3.1 Analysis method

Stress analyses were performed by using a FE analysis code (ANSYS Civil FEM 2012). Willam-Warnke concrete material model was employed to predict failure of concrete materials, for which corresponding ultimate tensile and compressive strengths were taken to define the failure surface.

$$\frac{F}{f_c'} - S \geq 0 \tag{1}$$

where F is a function of the principal stresses (σ_1, σ_2 and σ_3) and S is a failure surface expressed in terms of the principal stresses. Consequently, a failure limit of the concrete due to multiaxial stress state can be calculated. In a concrete element, cracking occurs when the principal tensile stress in any direction lies outside the failure surface. After cracking, the elastic modulus of concrete element is set to zero in the direction parallel to the principal tensile stress direction.

Failure determination of the reactor cavity and containment wall penetration is practically not easy because they consist of the liner plate and reinforced concrete that show complex ductile and brittle behaviors. In the previous study (Kim *et al*. 2016), two types of failures were defined; one is a failure of rebar and liner plate, which is associated with the exhaustion of material ductility of the steel. The other is a failure of concrete structures. The condition whether the reactor cavity and containment wall penetration fails or not was determined by structural FE analyses combined with damage evaluation. Particularly, for the rebar and liner plate made of carbon and austenitic stainless steels, a strain-based failure criterion was selected as the limiting value of 0.05 of which technical basis and rationale were described in NEI 07-13 (Nuclear Energy Institute 2011). On the other hand, for the concrete material, a stress-based failure criterion was derived. The cracking and crushing of concrete are closely related to ultimate tensile and/or compressive strengths which can be quantified by using failure ratio. If one of these failure criteria is violated, from a conservative point of view, it can be regarded as the loss of structural integrity of the reinforced concrete structure under the steam explosion conditions.

For the steel materials, a kinematic hardening model was adopted (ANSYS Civil FEM 2012, Olmati *et al*. 2013, Sadique *et al*. 2015) and a bi-linear elastic-plastic behavior was assumed. In this model, the strain rate dependent yield strength was defined as a function of several parameters as follows

$$f_y = \left[1 + \left(\frac{\dot{\varepsilon}}{C}\right)^{\left(\frac{1}{P}\right)}\right]\left(f_0 + \beta E_p \varepsilon_{eff}^p\right) \tag{2}$$

where f_0 is the yield strength, $\dot{\varepsilon}$ is the strain rate, C and P are the user defined Cowper-Symonds strain rate parameters, β is the hardening parameter, ε_{eff}^p is the effective plastic strain and E_p is the plastic hardening modulus which is given by

$$E_p = \frac{E_{tan}E}{E - E_{tan}} \tag{3}$$

where E is the modulus of elasticity and E_{tan} is the tangent modulus defined as the ratio of yield

strength and ultimate tensile strength at the failure strain.

3.2 Analysis conditions and material properties

Two kinds of vessel failure modes and locations such as SVF (Side Vessel Failure) according to focusing effect and BVF (Bottom Vessel Failure) center and side according to ICI (In-Core Instrumentation) tube failure locations were considered (Matjaž *et al*. 2015, OECD/CSNI/NEA 2006). As for corium conditions, specific temperatures (T^{cor}) of 3,150 K for the oxidation molten corium in the case of the BVF and 3,500 K for the metal molten corium in the case of the SVF were taken into account. Besides, the saturation temperature of coolant (T^{sat}) was determined as 273~304 K based on the corium conditions (Matjaž *et al*. 2016, Sehgal *et al*. 2005). In the previous study (Kim *et al*. 2015), pressure histories were determined and applied to discrete model A as loading conditions combined with gravitational loads of each component. In the present study, 3 cases of steam explosion conditions were considered as represented in Table 1 and Fig. 4.

Contact conditions were assigned inside of the reactor cavity and containment wall penetration. The liner plates were modeled as shell sharing nodes with the inner surface of the reactor cavity and containment wall penetration. The rebar was embedded in the concrete and the anchor bolts

Table 1 Steam explosion conditions (*Kim et al*. 2015)

Failure mode		Corium condition	
		T^{cor}	T^{sat}
BVF	ICI-center	3,150 K	304 K
	ICI-side	3,150 K	304 K
SVF		3,500 K	273 K

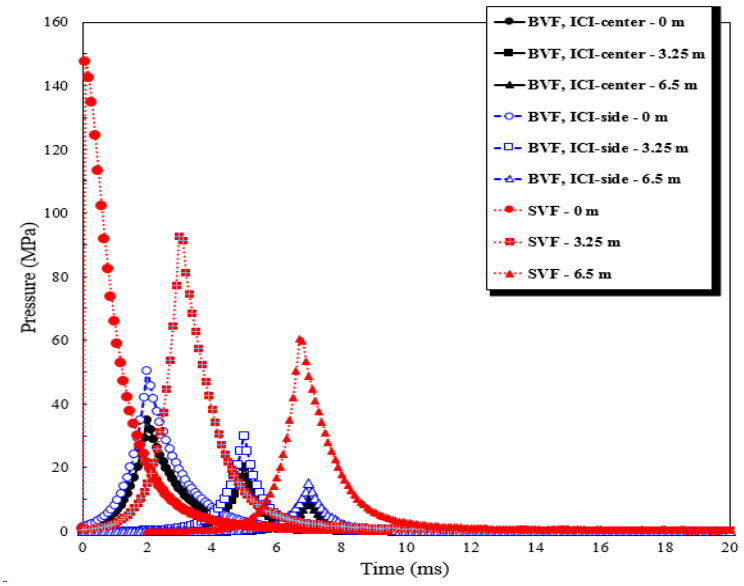

Fig. 4 Pressure histories of reactor cavity according to failure mode (Kim *et al*. 2015)

Table 2 Material properties

Component	E/f_{dy}	E_{tan}/f_{dy}	Poisson's ratio	f_{du}/f_{dy}
Concrete	530.2	623.60[1)]	0.2	0.056[2)]
Steel liner plate	573.8	8.84	0.3	1.500
Rebar	391.8	10.49	0.3	1.323
Anchor bolt	171.5	1.02	0.3	1.110
Reactor coolant piping, RPV	567.5	3.29	0.3	1.572
Head fitting and sleeve	666.9	17.48	0.3	1.697
Main steam piping, SG	379.3	8.84	0.3	1.659

[1)]: E_{tan}/f_{dc} (tangent modulus/compressive strength)
[2)]: f_{du}/f_{dc} (ultimate tensile strength/compressive strength)

were modeled by beam elements with equivalent diameters of the installed bolts per each support. As boundary conditions, bottom side of reactor cavity was fully fixed and each side of the containment wall penetration was fixed along the radial direction. Movement of each main steam piping was restricted by two support mechanisms as illustrated in Fig. 3. Equivalent spring stiffness values of upper support and lower support were 5.801×10^8 N/mm (*x*-direction) and 2.286×10^8 N/mm (*y*-direction).

Material properties were determined by considering DIF (Dynamic Increase Factor; 1.00~1.29) (ACI Committe 2010, Shokoohfar *et al*. 2016).

$$f_{dc} = f_c(DIF_c), \quad f_{dy} = f_y(DIF_y), \quad f_{du} = f_u(DIF_u) \tag{4}$$

where f_c, f_y and f_u are the compressive, yield and ultimate tensile strengths under static loading conditions, f_{dc}, f_{dy} and f_{du} are the compressive, yield and ultimate tensile strengths under dynamic loading conditions (Thai *et al*. 2015). Table 2 summarizes resultant material properties that were normalized by each yield strength of corresponding components.

4. Results and discussions

4.1 Analysis results

Figs. 5 and 6 compare stress distributions of discrete and integrated models under different failure modes and locations. To represent analysis results effectively, they were split into von Mises stress distribution of the steel components and radial stress distribution of reinforced concrete structures. The stresses were high at SVF conditions from the failure mode point of view. In Figs. 5(a) and (b), maximum von Mises stresses of discrete models occurred at bottom of RPV and main steam piping, respectively. In Figs. 6(a) and (b), maximum compressive stresses of discrete model occurred at bottom of reactor cavity and containment wall penetration while tensile stresses encompassed the compressive region along the radial direction. In addition, stress distributions were similar between the discrete models and integrated model as shown in Figs. 5(c) and 6(c). Particularly, the maximum stress also occurred at the bottom of reactor cavity that is the explosion location.

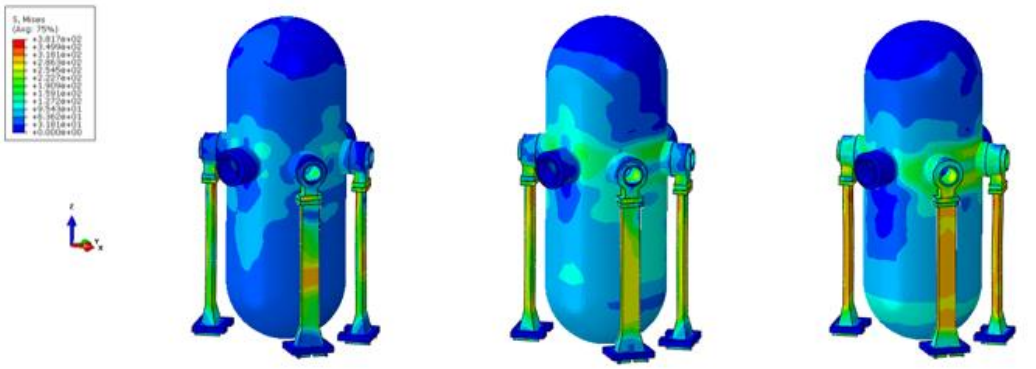

BVF, ICI-center BVF, ICI-side SVF

(a) Discrete model A

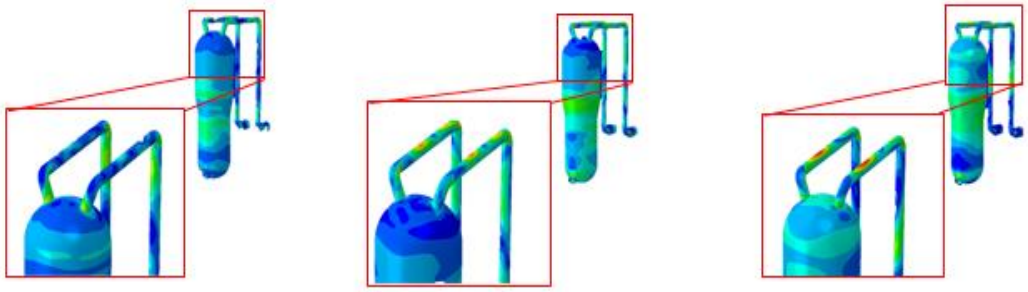

BVF, ICI-center BVF, ICI-side SVF

(b) Discrete model B

BVF, ICI-center BVF, ICI-side SVF

(c) Integrated model

Fig. 5 Comparison of von Mises stress distributions of steel components

Fig. 7 compares maximum von Mises stress values of the concrete, rebar and liner plate, which were normalized by yield strengths of each component. The differences between the discrete models and integrated model were not significant; almost the same in the discrete model A and

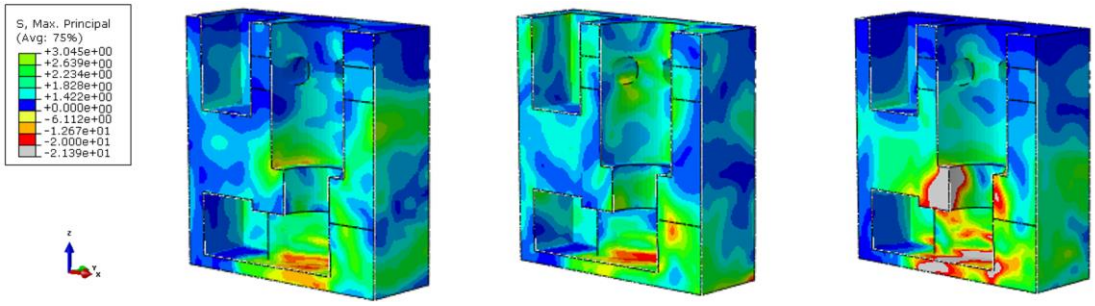

BVF, ICI-center BVF, ICI-side SVF

(a) Discrete model A

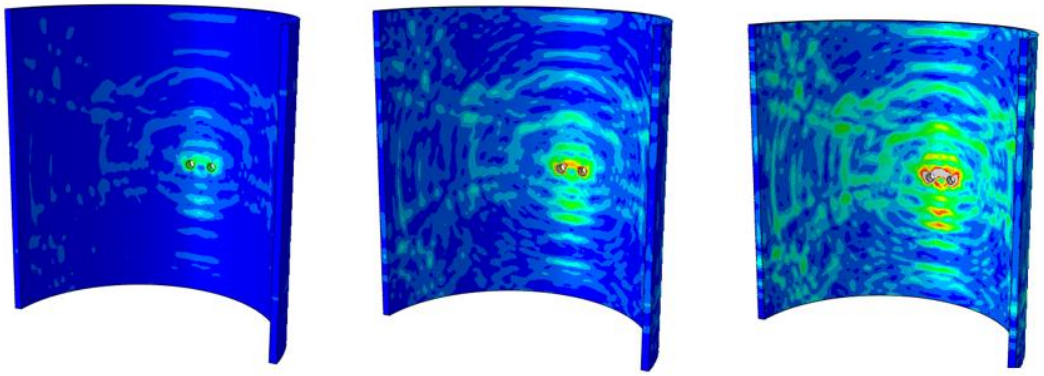

BVF, ICI-center BVF, ICI-side SVF

(b) Discrete model B

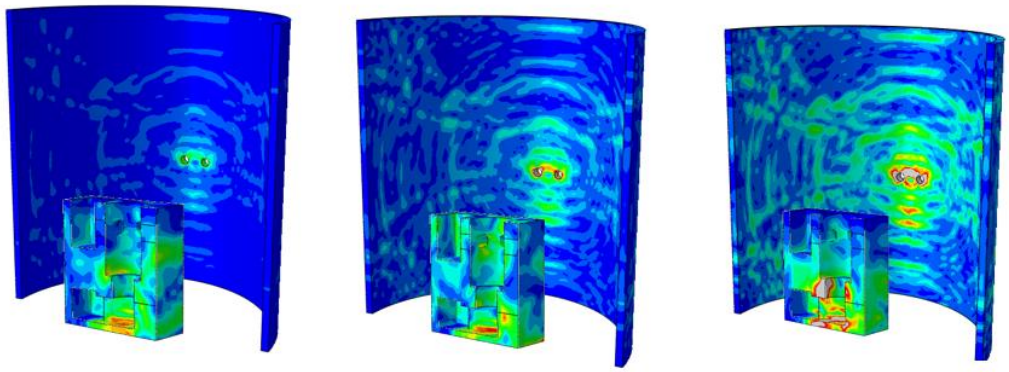

BVF, ICI-center BVF, ICI-side SVF

(c) Integrated model

Fig. 6 Comparison of radial stress distributions of reinforced concrete structures

less than 10% in the discrete model B. All the resulting von Mises stress values did not exceed the corresponding yield strengths except for some of the rebar and liner plate under SVF condition. Table 3 compares maximum equivalent strain values of the rebar and liner plate obtained from the discrete and integrated models. As summarized in the table, strains at the rebar under SVF

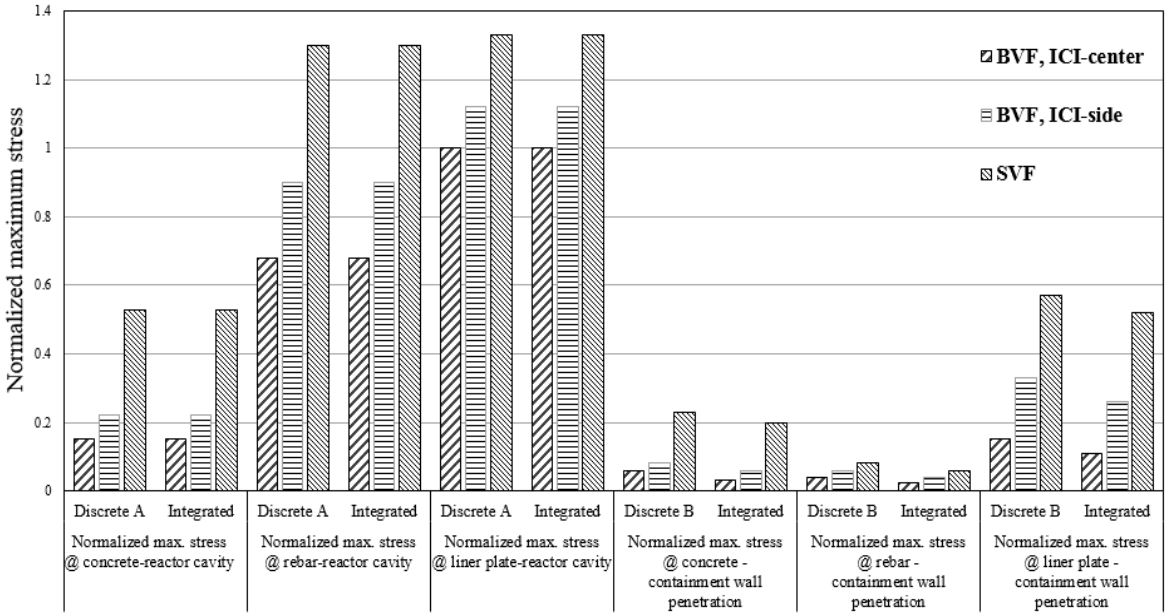

Fig. 7 Normalized maximum von Mises stresses of concrete, rebar and liner plate

Table 3 Maximum equivalent strains of rebar and liner plate

Failure mode and location		BVF		SVF
		ICI-center	ICI-side	
Max. equivalent strain @ rebar - reactor cavity	Discrete	0.023	0.024	0.031
	Integrated	0.023	0.024	0.031
Max. equivalent strain @ liner plate - reactor cavity	Discrete	0.018	0.019	0.021
	Integrated	0.018	0.019	0.021
Max. equivalent strain @ rebar - containment	Discrete	0.008	0.009	0.011
	Integrated	0.007	0.007	0.010
Max. equivalent strain @ liner plate - containment	Discrete	0.005	0.005	0.006
	Integrated	0.004	0.004	0.005

condition were higher than those at the liner plate under BVF conditions. However, all the resulting maximum equivalent strain values did not reach to the strain based failure criterion of 0.05. Moreover, Fig. 8 compares resulting normalized maximum stresses of other steel components. The von Mises stresses obtained from the discrete and integrated models were comparable within the maximum difference of 12% approximately. Also, the resulting stress values did not exceed the corresponding yield strengths so that material behaviors remained in elastic regime.

Table 4 represents maximum *y*-directional displacements of typical components such as the RPV and reactor coolant piping under different steam explosion conditions. The vertical movement of the RPV was less than 4.26 mm, which is quite small compared to the overall dimensions of the RPV. Meanwhile, damage evaluation of the reinforced concrete structures was

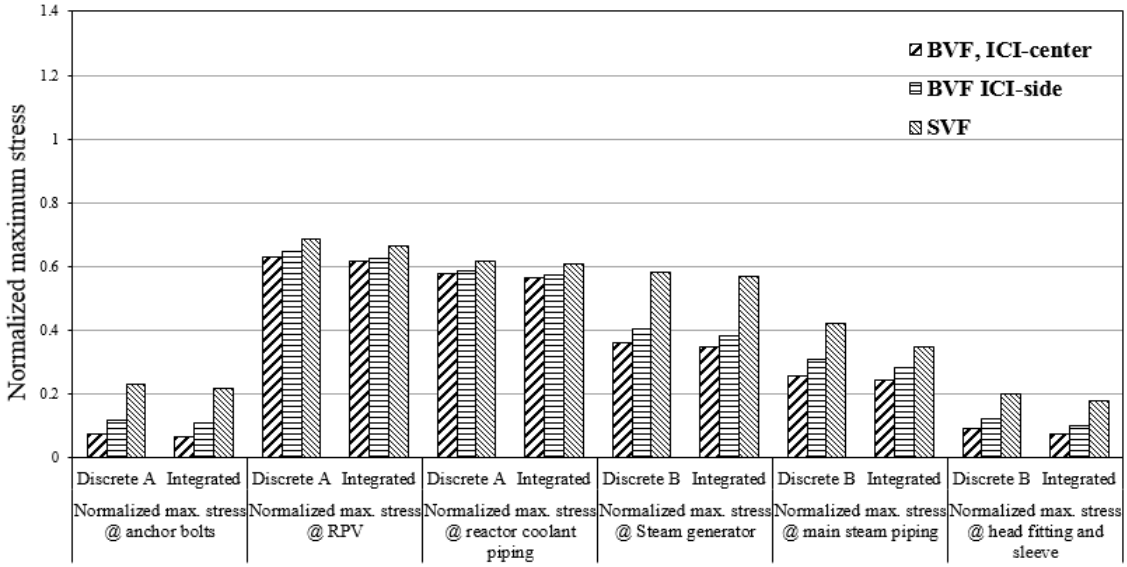

Fig. 8 Normalized maximum von Mises stresses of RPV, SG, piping and bolts

Table 4 Maximum *y*-directional displacements of RPV and reactor coolant piping

Failure mode and location		BVF		SVF
		ICI-center	ICI-side	
Max. displacement (mm) @ RPV	Discrete	2.01	2.58	4.26
	Integrated	1.54	2.01	3.69
Max. displacement (mm) @ reactor coolant piping	Discrete	1.74	2.12	3.95
	Integrated	1.22	1.68	3.29

performed by Willam-Warnke concrete material model. As depicted in Fig. 9, patterns and amounts of the cracking and crushing obtained from the discrete models and integrated model were almost the same. With regard to the reactor cavity, there were approximately 35%, 55% and 60% remained parts along the thickness under SVF, ICI-side and ICI-center respectively. With regard to the containment, there were minimum 92% remained parts even if the most severe condition of SVF was considered. The failure ratios of the concrete were 0.13 for the reactor cavity and 0.01 for the containment, which had sufficient margins comparing to the limiting value of 0.25 (Kim *et al*. 2016). Even though cracking and crushing occurred due to the steam explosion, integrity of the reactor cavity and containment wall penetration was ensured.

4.2 Discussion on structural integrity and damage evaluation

Effects of the RPV failure modes and locations due to the steam explosion were investigated, from which the SVF was determined as the most severe scenario. The difference of maximum stresses between SVF and BVFs was about three times, and the difference of maximum stresses between ICI-side and ICI-center was 30% approximately. However, the stresses generated at the all steel components were sufficiently lower than the corresponding yield strengths. The resulting

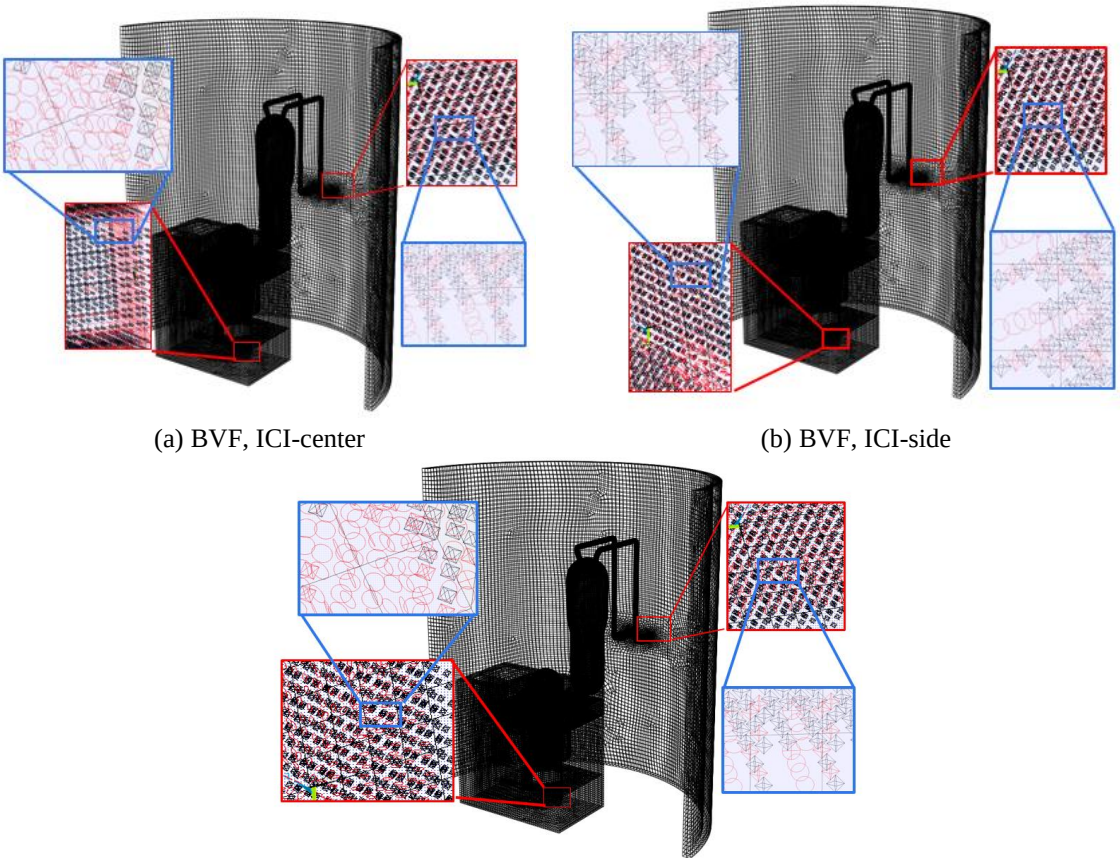

(a) BVF, ICI-center (b) BVF, ICI-side

(c) SVF

Fig. 9 Damage of reinforced concrete in integrated model

displacements showed similar trends, in general, and the vertical movements of major components were quite small compared to the overall dimensions of them.

Two failure criteria for the reinforced concrete structures such as the limiting failure ratio of concrete and the limiting strains for rebar and steel liner plate were satisfied under the steam explosion conditions. Even though cracking and crushing occurred mainly due to high pressure wave, reinforced concrete was not penetrated regardless of the failure modes and locations. In addition, the maximum equivalent strains of the rebar and steel liner plate were also less than the failure criterion specified in NEI 07-13 (Nuclear Energy Institute 2011). Overall, the analysis results between the discrete models and integrated model were not significant so that the latter is recommended as efficient and realistic model for steam explosion simulation.

In the present manuscript, pressure histories obtained from hydrodynamic analysis taking into account premixing, triggering and propagation phases, and CFD analysis considering explosion phase were applied to FE analyses sequentially (Kim *et al*. 2015). Moreover, two-way coupled simulation is being prepared in order to reflect concurrent interaction between fluid and structures. It is one of challenging issues to deal with further realistic behavior of steel components and reinforced concrete structures, of which results will be introduce in the near future.

5. Conclusions

In this study, a systematic structural assessment was carried out for nuclear steel components and reinforced concrete structures under typical steam explosion scenarios and the following conclusions were derived.

- The effect of failure modes on facilities was bigger than that of failure locations. While the highest stress was calculated at the reactor cavity under the SVF condition, its value was sufficiently lower than the corresponding yield strength.
- Two types of failure criteria were satisfied in all analysis cases. The equivalent strains of rebars and steel liner plates were less than the limiting value of 0.05 specified in NEI 07-13. Also, the reinforced concrete structures were not only penetrated by the cracking and crushing, but also the ratios of concrete failure were less than the limiting value of 0.25.
- FE analysis results between the discrete models and integrated model agreed well with the maximum difference of 12% so that the efficient and realistic integrated model was recommended for the steam explosion simulation.

Acknowledgements

This work was supported by the Nuclear Safety Research Program through the Korea Foundation Of Nuclear Safety (KOFONS), granted financial resource from the Nuclear Safety and Security Commission (NSSC), Republic of Korea (No. 1305001)

References

ACI Committee 349 (2010), Code requirements for nuclear safety related concrete structures, American Concrete Institute.

Chunyu, Z., Chen, P., Zhang, J., Lin, J., Liu, Y. Zhang, S. and Wang, B. (2014), "Evaluation of the structural integrity of the CPR1000 PWR containment under steam explosion accidents", *Nucl. Eng. Des.*, **278**, 632-643.

Cizelj, L., Koncar, B. and Leskovar, M. (2006), "Vulnerability of a partially flooded PWR reactor cavity to a steam explosion", *Nucl. Eng. Des.*, **236**, 1617-1627.

Cullis, I.G., Schofield, J. and Whitby, A. (2010), "Assessment of blast loading effects-Types of explosion and loading effects", *Int. J. Press. Ves. Pip.*, **87**, 493-503.

Hu, H.T. and Lin, Y.H. (2006), "Ultimate analysis of PWR prestressed concrete containment subjected to internal pressure", *Int. J. Press. Ves. Pip.*, **83**, 161-167.

Iqbal, A., Sadique, R., Bhargava, P. and Bhandari, N. (2014), "Damage assessment of nuclear containment against aircraft crash", *Nucl. Eng. Des.*, **278**, 586-600.

Kim, H.D., Kim, D.H., Kim, J.T., Kim, S.B., Song, J.H. and Hong, S.W. (2009), "Investigation on the resolution of severe accident issues for Korean nuclear power plants", *Nucl. Eng. Tech.*, **41**, 617-648.

Kim, S.H., Chang, Y.S., Song, S.C. and Cho, Y.J. (2015), "Structural assessment of fully flooded reactor cavity and penetration piping under steam explosion conditions", *Int. J. Press. Ves. Pip.*, **131**, 36-44.

Kim, S.H., Chang, Y.S., Song, S.C. and Cho, Y.J. (2015), "Structural assessment of main steam line and containment building under Steam Explosion Conditions", *Proceedings of the ASME PVP 2015 Conference*, PVP2015-45169.

Matjaž, L. and Uršič, M. (2015), "Analysis of PWR ex-vessel steam explosion for axial and side melt release", *Nucl. Eng. Des.*, **283**, 40-50.

Matjaž, L. and Uršič, M. (2016), "Ex-vessel steam explosion analysis for pressurized water reactor and boiling water reactor", *Nucl. Eng. Tech.*, **48**, 72-86.
Nuclear Energy Institute (2011), Methodology for performing aircraft impact assessments for new plant designs, NEI 07-13.
OECD/CSNI/NEA (2002), OECD lower head failure project final report.
Olmati, P., Petrini, F. and Bontempi, F. (2013), "Numerical analyses for the structural assessment of steel buildings under explosions", *Struct. Eng. Mech.*, **45**, 53-64.
Sadique, M.R., Iqbal, M.A. and Bhargava, P. (2015), "Crash analysis of military aircraft on nuclear containment", *Struct. Eng. Mech.*, **53**, 12-24.
Sehgal, B.R., Karbojian, A., Giri, A., Kymalainen, O., Bonnet, J.M. and Ikkonen, K. (2005), "Assessment of reactor vessel integrity", *Nucl. Eng. Des.*, **232**, 213-232.
Shokoohfar, A. and Rahai, A. (2016), "Nonlinear analysis of pre-stressed concrete containment vessel (PCCV) using the damage plasticity model", *Nucl. Eng. Des.*, **298**, 41-50.
Thai, D.K. and Kim, S.E. (2015), "Numerical simulation of reinforced concrete slabs under missile impact", *Struct. Eng. Mech.*, **53**, 43-54.
ANSYS Civil FEM (2012), Introduction of Civil FEM Ver. 14.0, ANSYS Inc.

CC